

Multi-spacecraft observations of the decay phase of solar energetic particle events

R. A. Hyndman¹, S. Dalla¹, T. Laitinen¹, A. Hutchinson^{2,3}, C. M. S. Cohen⁴, and R. F. Wimmer-Schweingruber⁵

¹ Jeremiah Horrocks Institute, University of Central Lancashire, Preston, United Kingdom
e-mail: rahyndman@uclan.ac.uk

² Heliophysics Science Division, NASA Goddard Space Flight Center, Greenbelt, MD 20771, USA

³ Goddard Planetary Heliophysics Institute, University of Maryland, Baltimore County, Baltimore, MD 21250, USA

⁴ California Institute of Technology, Pasadena, CA 91125, USA;

⁵ Institute of Experimental and Applied Physics, Christian-Albrechts-University Kiel, Leibnizstraße 11, 24118 Kiel, Germany

Received Month Day, Year; accepted Month Day, Year

ABSTRACT

Context. Parameters of solar energetic particle (SEP) event profiles such as the onset time and peak time have been researched extensively to obtain information on acceleration and transport of SEPs. Corotation of particle-filled magnetic flux tubes with the Sun is generally thought to play a minor role in determining intensity profiles. However recent simulations have suggested that corotation has an effect on SEP decay phases, depending on the location of the observer with respect to the active region (AR) associated with the event.

Aims. We aim to determine whether signatures of corotation are present in observations of decay phases of SEP events and study how the parameters of the decay phase depend on the properties of the flares and coronal mass ejections (CMEs) associated with the events.

Methods. We analyse multi-spacecraft observations of SEP intensity profiles from 11 events between 2020 and 2022, using data from SOLO, PSP, STEREO-A, and SOHO. We determine the decay time constant, τ , in 3 energy channels; electrons ~ 1 MeV, protons ~ 25 MeV, and protons ~ 60 MeV. We study the dependence of τ on the longitudinal separation, $\Delta\phi$, between source AR and the spacecraft magnetic footprint on the Sun.

Results. Within individual events there is a tendency for the decay time constant to decrease with increasing $\Delta\phi$, in agreement with test particle simulations. The magnitude of the event as measured through the intensity of the associated flare and SEP peak flux have an effect on the measured τ values and are likely the cause of the observed large inter-event variability along with varying solar wind and interplanetary magnetic field conditions.

Conclusions. We conclude that corotation has a significant effect on the decay phase of a solar energetic particle event and should be included in future simulations and interpretations of these events.

Key words. SEPs, Sun: Corotation, SEPs: Decay phases

1. Introduction

Solar energetic particles (SEPs), accelerated by shocks driven by coronal mass ejections (CMEs) and during flares, in gradual and impulsive events respectively, are detected as sporadic increases of particle intensities up to and past 1 au from the Sun (Klein & Dalla 2017) by spacecraft in interplanetary space. Typical SEP time-intensity profiles have a rise phase, a peak intensity, and a decay phase. Decay phases, from peak to background levels, can last anywhere between a few hours to several days (Van Allen & Krimigis 1965).

Historically, the analysis of SEP profiles has been based on one spacecraft observing many events from different source locations on the Sun. This allows investigation into how source location affects time profiles (Cane et al. 1988), however, this kind of study cannot separate differences caused by observer location from those caused by the fact that events are produced by different solar eruptions, and that solar wind and interplanetary magnetic field (IMF) conditions vary from event-to-event.

Presently we are in a golden era of SEP research, with multiple spacecraft capable of taking simultaneous SEP measurements in different locations in interplanetary space. This al-

lows us to compare profiles seen in different locations from the same source active region (AR), reducing effects from parameters which change event-to-event. Multiple spacecraft around the Sun also allows for more frequent particle observations as with more spacecraft there is a higher chance that an event will be observed (Rodríguez-García et al. 2024).

Decay phases of SEP events were originally thought to be indicative of the turbulence-induced scattering experienced by SEPs in interplanetary space before reaching the observer. It was thought that longer decay phases resulted from stronger scattering conditions, and shorter decay phases resulted from weaker scattering conditions. A value for the scattering mean free path was derived by fitting the intensity profile (Kallenrode et al. 1992) as modelled via 1D focussed transport. The gradual and impulsive scheme for events came about in the 1990's, linking acceleration of SEPs to CME-driven shocks for gradual events. The duration of the decay phase for gradual events has since been thought to be related to time-extended shock acceleration, especially at low energies, such that a longer acceleration leads to a longer duration of the decay phase (Reames et al. 1996).

In addition to turbulence and acceleration duration, solar rotation can also affect the temporal profile of an SEP event. The

outward flow of the solar wind from the Sun generates magnetic flux tubes that are wound into the Parker spiral by the Sun's rotation. As the Sun spins, the magnetic flux tubes also rotate with the Sun from the east to the west. This effect is referred to as corotation (McCracken et al. 1971). From an intuitive point of view, one would expect some effects of corotation on SEP intensity profiles. Neglecting significant cross-field diffusion, once SEPs are injected into space, corotation causes particle-filled magnetic flux tubes to be 'pulled' along towards the west over time, relative to an observer. This means that when an observer views an event from an eastern source region the filled flux tubes are rotating towards them, and when an observer views a western event the filled flux tubes are rotating away from them. This would affect the decay phase, with western events in particular being cut short. If corotation has a significant effect on decay phases of SEP events, this east-west difference should be visible in comparisons of decay phase duration against observer location.

Some studies have included corotation such as Giacalone & Jokipii (2012) and Laitinen et al. (2018). Giacalone & Jokipii (2012) simulated impulsive events and included corotation through the movement of field lines over time. They stated that rotation of the field line, along with other transport effects, allows these compact events to be seen at wide longitudes. Laitinen et al. (2018) used a simple 1D diffusion model to simulate SEP propagation from a flare-like injection, and compared simulations with and without corotation. They concluded that corotation affects the event profiles, citing decay phase and intensity differences at different longitudes with respect to source ARs. Daibog et al. (2006) used single-spacecraft observations to investigate the effects of observer longitude on proton intensity profiles. They concluded that the trend they observed is due to the rotational effect discussed in McCracken et al. (1971).

However, in the study and modelling of gradual SEP events the role of corotation is usually neglected. This is based upon the results of 1D focussed transport models that included corotation in an approximate way (Lario et al. 1998; Kallenrode & Wibberenz 1997) and concluded it has negligible effects. Reames et al. (1997) also concluded it does not play an important role, by analysing a few SEP events displaying spatially and temporally invariant spectra.

Recent 3D test particle modelling of SEPs injected by a wide shock-like source has suggested that corotation has a significant effect on the decay phases of SEP events. Hutchinson et al. (2023a) ran simulations of SEP propagation which modelled particle transport with and without corotation. They found that including corotation had a notable effect on decay phases with the decay time constant τ displaying a dependence on the longitudinal separation between source active region and observer footpoint (their Figure 3).

Lario (2010) used single-spacecraft observations to investigate decay phases of near relativistic electron events. Figure 10 in their paper analysed the dependence of τ on source AR longitude. They did not find any dependence of τ on source AR longitude in their dataset.

This work aims to investigate SEP decay phases during 11 multi-spacecraft events. We use data from 4 spacecraft: Solar Orbiter (SolO), the Parker Solar Probe (PSP), the Solar and Heliospheric Observatory (SOHO), and the Solar TERrestrial RElations Observatory - Ahead (STEREO-A). We analyse data for protons and electrons and fit the intensity profiles to obtain the value of the decay time constant τ . We analyse the dependence of τ on the relative location between observers and the source AR of the event, as well as the parameters of the solar events ac-

celerating the particles. We aim to investigate possible signatures of corotation and compare any results to those of the simulations of Hutchinson et al. (2023a).

In Section 2 we discuss the methodology used to find decay time constant values for the measured intensity-time profiles. In Section 3 we present our results, comparing τ values with the locations of the observing spacecraft relative to the active region and the parameters of each event. In Section 4 we present our conclusions.

2. Data and Methodology

2.1. Data Sources

We use data from SolO (Müller et al. 2020), PSP (Fox et al. 2016), SOHO (Domingo et al. 1995) and STEREO-A (Kaiser et al. 2008) to create SEP multi-spacecraft intensity-time plots. The instruments used for each are: SolO High Energy Telescope (HET) (Rodríguez-Pacheco et al. 2020), PSP Integrated Science Investigation of the Sun (IS \odot IS/EPI-Hi/HETA) (McComas et al. 2016), SOHO Energetic and Relativistic Nuclei and Electron experiment (ERNE) (Torsti et al. 1995; Valtonen et al. 1997) and Electron Proton Helium INstrument (EPHIN) (Müller-Mellin et al. 1995), and STEREO-A High Energy Telescope (HET) (von Rosenvinge et al. 2008).

We chose to use multiple energy channels to determine if there were any differences in our results based on particle species or energy. The energy channels of the different instruments do not overlap exactly. For our multi-spacecraft analysis we identified channels with similar ranges for protons around 25 MeV and 60 MeV (see Table 2). For electrons we used channels with ranges around 1 MeV. In Table 2 the relevant spacecraft instruments and energy channels used for different particle species are listed. Particle intensities are given in standard units for all spacecraft and channels except for the PSP/IS \odot IS electron \sim 1 MeV channel, where count rate data was used. The count rate data for the PSP channels that cover the range between 0.6 and 1.2 MeV are summed to obtain a 0.6 - 1.2 MeV channel that is more comparable to the other instruments' channel widths. This was the only channel that was formed from several channels summed together. All data were downloaded using the SERPENTINE analysis tools (Palmroos et al. 2022). SOHO, STEREO-A, and SOLO data are at a 30 minute cadence, while PSP data are available at a 60 minute cadence.

2.2. Event Selection

We selected events between 2020 and 2022 based on the availability of multi-spacecraft data. An event was selected for study if:

- at least two spacecraft had observed the event in at least one of the energy channels used.
- observing spacecraft were at radial distance was further than 0.6 au from the Sun. This is to ensure that only a relatively small range of distances are used, to ensure similar transport conditions, and to avoid events close to the Sun where spacecraft are moving fast across longitudes, which may influence profiles.
- the observations had reliable count rate/intensity-time data. This required the observations to have no significant gaps in the data, such that fits to the decay phase were within the goodness-of-fit requirements discussed in Section 2.3.
- any events occurring before or after the chosen event could be separated from the decay phase of the event being studied.

The 11 events selected are listed in Table 1.

2.3. Decay Time Constant

In order to quantify the decay phase of the SEP events analysed in this study, we define the decay time constant, τ , as:

$$\tau = - \left(\frac{d(\ln I)}{dt} \right)^{-1} \quad (1)$$

where I is the particle intensity and t is time.

To derive τ , we start by removing background intensities. We average the background intensities over twenty hours, from one day to 4 hours prior to the event start time. In the case that this time frame includes previous events, we instead select a twenty hour time frame when the intensities are at background level before all the events. We take the mean of the background intensities during these times and subtract the mean from the data from each instrument.

We then use `scipy.stats.linregress`¹ to fit a straight line to the decay phase on logarithmic intensity-time plots. The period that is used to fit the decay phase starts from the time when the intensity value falls to 90% of the peak intensity, I_p , and ends when particle intensities reach background levels again (or until a following event is detected). We fit from 90% of the I_p value, instead of from the I_p itself, so that we avoid our measured decay phase beginning too early. In some profiles, intensities plateau at the I_p for a time before decaying begins, so requiring the intensity to drop by 10% allows us to get a more accurate decay phase duration. Given that for PSP electrons we are combining four channels to derive a synthetic channel at energy 0.6-1.2 MeV, we have checked the values of the decay time constant for the four individual channels and we have found that, for the events analysed, the decay time constant is very similar for each of the four channels.

To evaluate the goodness-of-fit for each decay slope we use the p-value returned by `scipy.stats.linregress`. This is the p-value for a hypothesis test using the Wald Test where the slope of the regression line is less than zero. A fit is accepted so long as the p-value of the fit is ≤ 0.05 and the fit is over at least 9 hours. The minimum time limit was set to allow for a significant number of points for analysis as most data were at a 30 minute cadence (SOLO, SOHO, and STEREO data). Fits with more than 18 points were judged as accurate using the goodness-of-fit p-value and also by eye. 18 points were also required for the PSP data, although this corresponds to 18 hours as these were 60 minute averaged data. Previous studies on the decay phase also place time limits on decay phases to be included in analysis: for example, Daibog et al. (2006) take 12 hours as their lower limit. After fitting a straight line to the decays, the gradients of the straight lines are converted to the decay time constant values, τ , using Equation 1.

The error bars are calculated from values given by the fitting routine. The maximum and minimum values for the decay phase's fit are converted to hours using Equation 1 and added to each point. The maximum slope value corresponds to the lowest τ value, and the minimum slope value corresponds to the highest τ value.

For some of the SEP intensity profiles, the decay seems to have two phases. Lario (2010) noted that some SEP events have two decay phases where the earlier stage follows a power-law and the later stage follows an exponential decay. Lario

(2010) found that observations of one-phase decays were mostly found outside the nominal well-connected longitudes. To verify whether the presence of two-phase decays affects the τ values significantly, we also ran our fitting routine starting the fit when the intensities reach 50% of I_p to background. This allowed us to obtain τ values focussing only on late decay. This is discussed further in Section 3.5.

2.4. Solar Event Properties

Source ARs of the solar events associated with the SEP event were obtained from the SERPENTINE Events Catalogue (Dresing et al. 2024). Longitude values of the ARs were taken from the catalogue as well as the associated CME speeds, flare classes, and maximum peak particle flux for the ~ 25 MeV proton channel, $I_{p,25}^{max}$, for the events. (CME speed and flare class values in the catalogue originally come from LASCO and GOES respectively).

To characterise observer location with respect to the event's source AR, we define $\Delta\phi$, the difference in longitude between the observer's magnetic footpoint on the Sun, and the event's associated AR as:

$$\Delta\phi = \phi_{AR} - \phi_{f1pt} \quad (2)$$

where ϕ_{AR} is the longitude of the source AR, and ϕ_{f1pt} is the longitude of the observer's magnetic footpoint on the Sun. We find the ϕ_{f1pt} for each spacecraft using the open-source tool Solar Magnetic Connection HAUS (Solar-MACH) (Gieseler et al. 2023). ϕ_{f1pt} is calculated using the nominal Parker Spiral for each spacecraft based on the solar wind speed, V_{sw} . V_{sw} is taken from Coordinated Data Analysis Web (CDAWeb)². The V_{sw} value observed closest to the event start time, and within two hours of the start time, is used. Event start times are taken from the SERPENTINE Events Catalog (2024). Where V_{sw} data are not available within two hours of the event's start time, we use 450 kms^{-1} as a default value.

When the AR is to the west of the footpoint of the spacecraft (western events), $\Delta\phi > 0$, and when the AR is to the east of the footpoint of the spacecraft (eastern events), $\Delta\phi < 0$.

3. Results

3.1. Decay time constant against longitudinal separation

In Figure 1 we plot the decay time constant, τ , against $\Delta\phi$ for ~ 25 MeV protons for 10 events. The 2022-02-15 event is not included for the reasons discussed in Section 3.3. Each event is colour-coded, with solid lines connecting the points contributed from each observing spacecraft. The grey shaded area indicates the dependence of τ on $\Delta\phi$ that is obtained from 3D test particle simulations for 25 MeV protons when corotation is included. The dependence was obtained by using similar simulations to those by Hutchinson et al. (2023a,b) who ran 3D test particle simulations of SEPs injected from a shock-like source and propagated a mono-energetic (5 MeV) proton population for 72 hours. In the present work we have run 3D test particle simulations for 25 MeV protons, keeping all other parameters the same as in Hutchinson et al. (2023b) and obtained the grey shaded area on Figure 1.

We can see in Figure 1, that for a given $\Delta\phi$ value, a broad range of τ values are observed. In general, a larger spread and

¹ <https://www.nature.com/articles/s41592-019-0686-2>

² <https://cdaweb.gsfc.nasa.gov>

Event Date	Flare Time (UTC)	Flare Location (Stonyhurst, [lon., lat.], °)	Flare Class	CME Speed (kms ⁻¹)	Peak Flux, $I_{p,25}^{max}$ (cm ⁻² s ⁻¹ sr ⁻¹ MeV ⁻¹)
29-11-20	12:34:00	[-82.0, -23.0]	M4.4	2077	4.64e+00
07-12-20	15:46:00	[8.2, -25.0]	C7.4	1407	7.11e-02
28-05-21	22:19:00	[54.9, 19.0]	C9.4	971	2.35e-01
09-06-21	11:50:00	[89.0, 27.0]	C1.7	441	9.28e-02
09-10-21	06:19:00	[-8.3, 18.0]	M1.6	712	3.32e-01
28-10-21	15:17:00	[1.2, -28.0]	X1.0	1519	5.13e+01
20-01-22	05:41:00	[75.8, 8.0]	M5.5	1431	2.45e-01
15-02-22	21:50 UT*	[-134.0, 33.0]*	-	1905	7.13e+00
14-03-22	17:13:36	[109.0, -24.0]	B8.5	740	9.04e-02
28-03-22	10:58:00	[4.3, 14.0]	M4.0	905	6.65e-01
11-05-22	18:08:00	[89.3, -17.0]	M2.7	1100	5.19e-02

Table 1: Associated flare and CME properties for SEP events analysed. Event date and flare onset time and location are given. These times and locations are taken from the SERPENTINE Events Catalog (Dresing et al. 2024). Entries marked with * are taken from Khoo et al. (2024) rather than the SERPENTINE catalogue due to data availability. Event magnitude proxies such as flare class, CME speed and maximum peak flux, $I_{p,25}^{max}$ values are given. Flare classes and $I_{p,25}^{max}$ values are also taken from SERPENTINE. $I_{p,25}^{max}$ values are the maximum proton peak flux for the \sim mb channel, across the 4 observing spacecraft we use. CME speeds are plane of sky speeds from LASCO. Where more than one CME is associated, the largest plane of sky LASCO value is used.

Instrument	Solo HET	PSP IS \odot IS	SOHO ERNE	SOHO EPHIN	STEREO-A HET
Electrons \sim 1 MeV	1.05-2.40	0.6-0.7	N/A	0.67-10.4	0.7-1.4
		0.7-0.8			
		0.8-1.0			
		1.0-1.2			
Protons \sim 25 MeV	25.09-27.20	26.9-32.0	25-32	25-53	26.3-29.7
Protons \sim 60 MeV	63.10-68.97	N/A	64-80	N/A	60-100

Table 2: Energy channels used for multi-spacecraft analysis. For electrons, count rates in the 4 PSP channels shown were summed.

higher τ values are seen for eastern events ($\Delta\phi < 0$) compared to western events ($\Delta\phi > 0$). Considering each event individually, one can see that there is a tendency for τ to decrease as one moves from east to west for most of the events. This agrees with the trend from the test particle simulations.

To capture the east-west trend, in Figure 2 we show the best linear fit to the data points corresponding to an individual event for the proton \sim 25 MeV channel. We call the gradient of these fits $\frac{d\tau}{d(\Delta\phi)}$ and they are shown as colour-coded dashed lines on Figure 2.

We plot $\frac{d\tau}{d(\Delta\phi)}$ of each event against CME speed in Figure 3. It can be seen that almost all events have negative gradients, supporting the hypothesis of higher τ values in the east and lower τ values in the west. Two events have positive gradients, but both of these values are small. On the whole, a trend for higher eastern τ values and lower western τ values is seen.

Our focus has been on the \sim 25 MeV proton channel as it has the largest number of measurements available. However data for other channels have also been analysed. Decay time constant versus $\Delta\phi$ plots for \sim 1 MeV electrons and \sim 60 MeV protons are seen in Figures 4 and 5 respectively. The \sim 1 MeV electron

channel and the \sim 60 MeV proton channel display similar trends to those seen for \sim 25 MeV protons, with fewer data points.

Figure 4 shows that the \sim 1 MeV electrons have higher τ values than the \sim 25 MeV protons for some events, and lower values for others, giving a larger spread in values for this particle species, while maintaining a general east-to-west decrease trend for each event. This could mean that corotation affects electrons to a different degree that it affects protons, although it could also point to other factors which may affect τ values for electrons differently to protons. These other factors are discussed in Section 3.2.

Values of τ for the \sim 60 MeV proton channel tend to be slightly lower than those for the \sim 25 MeV channel for the same observer, and event, indicating a faster decay at higher energy. In the \sim 60 MeV proton channel, there are far fewer data points available than in the other channels analysed. One reason for this is that intensities are lower in this higher energy channel meaning that decay phases are more difficult to fit with adequate statistics. Lower peak intensities also mean that background levels are reached earlier and the decay phase is cut off. There is no \sim 60 MeV proton data available from the PSP IS \odot IS/EPI-Hi instrument leading to fewer available measurements at this energy. Another reason for fewer data points is that lower magnitude so-

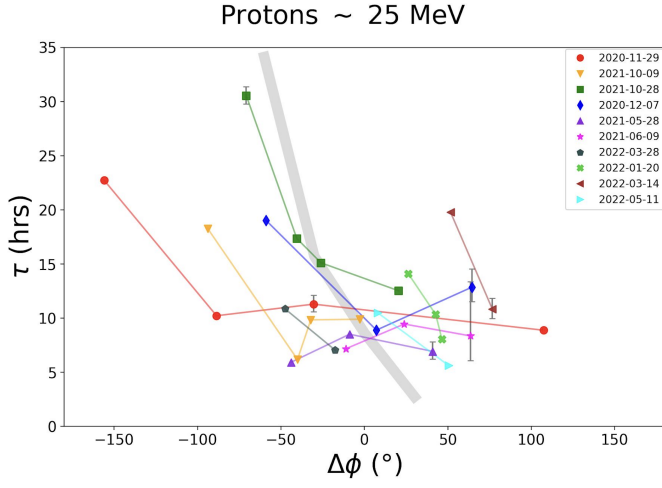


Fig. 1: Decay time constant τ versus longitudinal separation $\Delta\phi$ (as given by Equation 2) for protons at ~ 25 MeV. Coloured lines connect s/c data points for a single event. Grey shading show results from a 25 MeV simulation run following the methodology of Hutchinson et al. (2023b). Error bars are omitted when they are smaller than the data points.

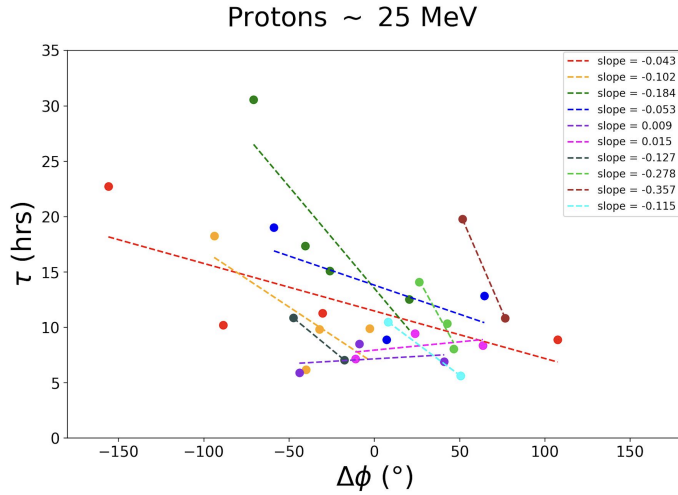


Fig. 2: τ against $\Delta\phi$ with each event in a different colour. Best-fit dashed lines are plotted for each event and the gradient values ($hrs/^\circ$) of these lines can be seen in the key.

lar events (as measured with proxies such as flare class, CME speed, and SEP peak flux) do not accelerate particles to this energy. Higher magnitude events may accelerate particles to higher energies, however these high energy particles may decelerate or escape to greater radial distances than the spacecraft location before reaching a spacecraft at large $|\Delta\phi|$. Alternatively, the flanks of the shock may not accelerate particles as efficiently as the nose of the shock at the higher energies resulting in a smaller number of events. All these reasons may explain the lack of points at large $|\Delta\phi|$ in Figure 5.

3.2. Comparing Two Events with Similar Geometries

A key characteristic that plays a role in determining the value of τ is the overall magnitude of the solar eruptive event that accelerated the particles. An example of this can be seen in the following case study of two events with very similar geometries.

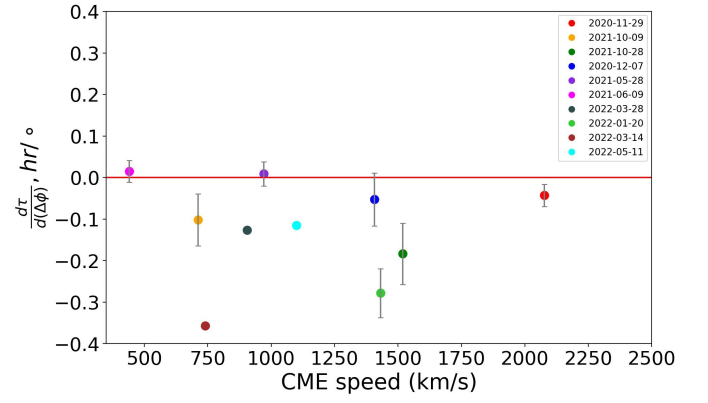


Fig. 3: $\frac{d\tau}{d(\Delta\phi)}$ values from the linear fit of τ vs $\Delta\phi$ data points for each event, against CME speed. Red line marks the gradient = 0 line.

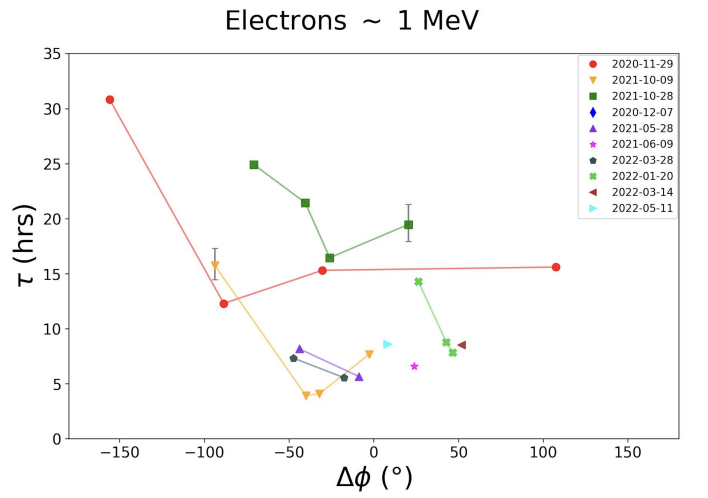


Fig. 4: Decay time constant τ versus longitudinal separation $\Delta\phi$ (as given by Equation 2) for electrons at ~ 1 MeV. Coloured lines connect s/c data points for a single event. Error bars are omitted when they are smaller than the data points.

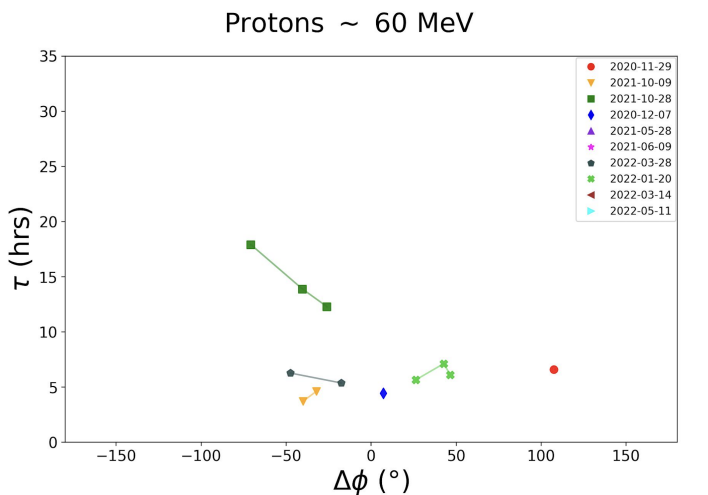


Fig. 5: Decay time constant τ versus longitudinal separation $\Delta\phi$ (as given by Equation 2) for protons at ~ 60 MeV. Coloured lines connect s/c data points for a single event. Error bars are omitted when they are smaller than the data points.

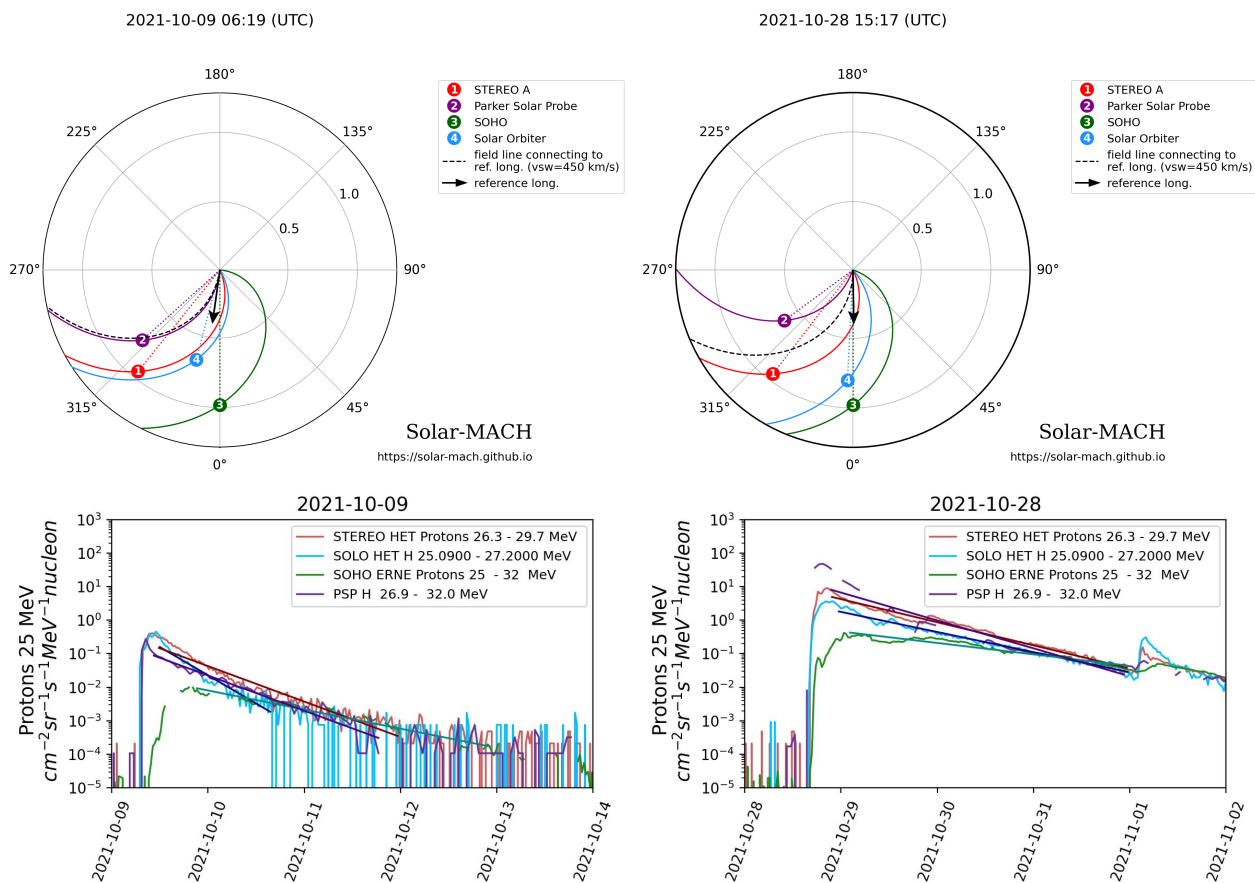


Fig. 6: Spacecraft configurations (top panels) and SEP intensity profiles (bottom panels) for the two case study events: 09-10-2021 (left) and 28-10-2021 (right). The spacecraft configurations are from Solar-MACH with colour-coded circles indicating the spacecraft locations and nominal Parker spirals calculated from measured solar wind speed at the spacecraft. Multi-spacecraft SEP intensity profiles for the proton ~ 25 MeV channel have been made using SERPENTINE tools. The 28-10-2021 event’s decay is cut off due to a second event occurring on the 01-11-2021.

The events of 9 October 2021 and 28 October 2021 took place less than a month apart and the observing spacecraft moved very little in that time. Therefore, the locations of the spacecraft are very similar for the two events (see Figure 6 top panels). This combined with the fact that the locations of the source ARs are close to each other in longitude (2021-10-09: E08N18 (Stonyhurst), 2021-10-28: W01S28), means that the $\Delta\phi$ values are very similar.

If the geometrical locations were the only influence on τ value, we would expect the events to have similar values of τ for each spacecraft. However, as seen in Table 3 which shows the τ values for each spacecraft and channel for the two events, the τ values for the 28 October 2021 event are much larger than those for the 9 October 2021 event. We see this also in the comparison of the events in Figure 1 (yellow triangles and green squares).

The reason for these differing τ values may lie in the difference in magnitude of the events. 2021-10-09 is an M1.6 class flare event, while 2021-10-28 is an X1.0 class flare event. The events also have differing CME speeds, with 2021-10-09 having an associated CME plane of sky (POS) speed of 712 km/s while 2021-10-28 has CME POS speed of 1519 km/s. SEP peak flux for protons ~ 25 MeV, $I_{p,25}^{max}$, for the events also differs, at around $3.32 \times 10^{-1} \text{ cm}^{-2} \text{ s}^{-1} \text{ sr}^{-1} \text{ MeV}^{-1}$ for 2021-10-09, and the $5.13 \times 10^1 \text{ cm}^{-2} \text{ s}^{-1} \text{ sr}^{-1} \text{ MeV}^{-1}$ for 2021-10-28. All three of these parameters can be used as proxies for the magnitude of

the events. Overall, 2021-10-09 is much less energetic than the 2021-10-28 event.

More energetic solar events are capable of accelerating particles up to higher energies than less energetic events, and there are many more particles at the high energies in more energetic events, so we can see them above background for a longer time. This could result in extended decays, in particular for lower energy channels, caused by particles with higher energies decelerating and filling these lower channels as time goes on. More energetic events may also accelerate more particles over longer times causing extended decay phases. The 2021-10-28 event was able to accelerate particles to much higher energies than the 2021-10-09 event, as demonstrated by the detection of an associated ground level enhancement (GLE) event, showing that it accelerated protons to energies > 500 MeV.

In addition, more intense events tend to fill a broader region of the heliosphere with particles and this, with the corotation effect, would result in longer decay phases for more intense events. We conclude that the larger τ values in the 2021-10-28 event are a result of the overall event magnitude being much larger than for the 2021-10-09 event. Thus, the observed large variation in τ values seen in Figure 1 could be due to the parameters which vary between events such as solar event magnitude (as measured by flare class, CME speed, and peak intensity). Solar wind and IMF conditions are expected to play a role as well.

2021-10-09	SOLO	STEREO-A	SOHO	PSP
Electrons ~ 1 MeV	3.9	4.1	15.8	7.8
Protons ~ 25 MeV	6.2	9.9	18.3	9.9
Protons ~ 60 MeV	3.7	4.6	NaN	NaN

2021-10-28	SOLO	STEREO-A	SOHO	PSP
Electrons ~ 1 MeV	21.5	16.5	24.9	19.5
Protons ~ 25 MeV	17.4	15.1	30.6	12.5
Protons ~ 60 MeV	13.9	12.3	17.9	7.8

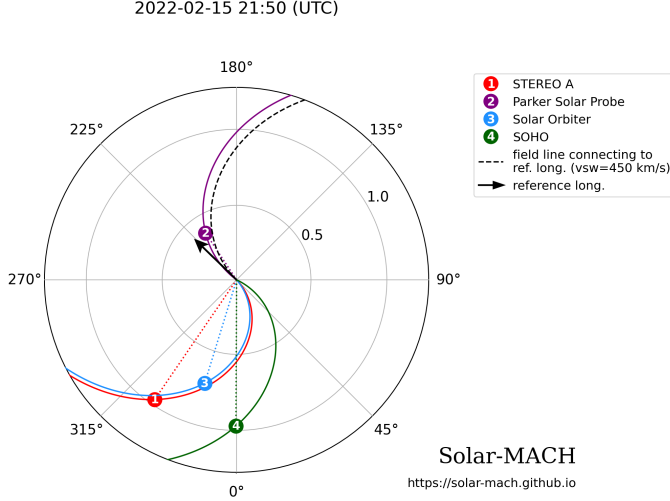
 Table 3: τ values, in hours, for case study events.


Fig. 7: Solar-MACH plot for 2022-02-15. Longitudes are in Stonyhurst coordinates. Spacecraft locations and nominal Parker spirals are colour-coded as seen in key. Parker spirals are calculated using the solar wind speeds measured by each spacecraft. The black arrow shows the location of the source AR, and the black dotted line shows the nominal Parker spiral for that location assuming a solar wind speed of 450 km/s.

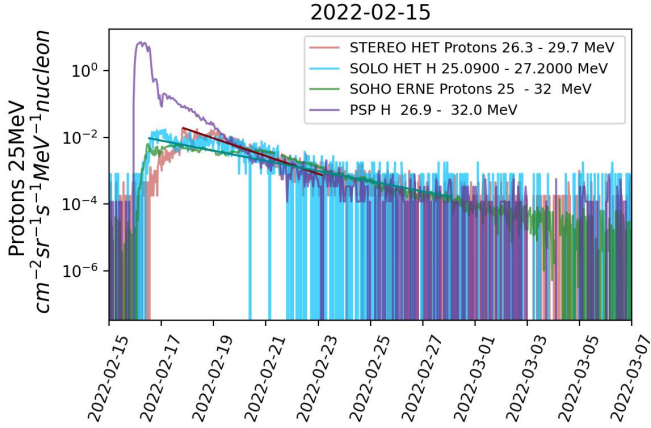


Fig. 8: Intensity profiles for the proton ~ 25 MeV channel for the 2022-02-15 event.

3.3. Wide angular separation event: 2022-02-15

An event on 2022-02-15 was studied but not included in Figures 1-5. The flare location and flare time for this event are taken from Khoo et al. (2024). Four spacecraft observe the event, and their geometry can be seen in Figure 7. PSP is well-connected with $\Delta\phi = -8.5$, but is closer to the Sun than we allow for our analysis

($r = 0.38$ AU). The other three spacecraft are connected to the far side of the Sun with respect to the source AR with $\Delta\phi = -179.0^\circ$, -175.5° , 160.4° for STEREO-A, SOLO and SOHO respectively.

The profiles for the ~ 25 MeV channel for the four observing spacecraft can be seen in Figure 8. Of the three spacecraft at the far eastern and far western longitude separations, only the STEREO-A and SOHO measurements met our fitting requirements in the ~ 25 MeV proton channel. The STEREO-A τ value was 39.2 hours and the SOHO τ value was 68.5 hours. Given that the $\Delta\phi$ values for the spacecraft are -179.0° and 160.4° , these τ values would place points beyond the top left and top right hand corners of Figure 1 respectively. The SOHO τ value in particular may be affected by fluctuations around the peak value as seen in Figure 8.

Figure 8 shows that for these wide angular separation events, the rise and peak phase extend over several days such that the uncertainty in the values of τ is large. We note that the τ values in this event are much larger than those in Figure 1, with the value at SOHO being more than double the maximum τ value of any other event. In addition, for this event we only have 2 points, both at wide longitudinal separations, given that PSP was too close to the Sun for inclusion in our analysis. For these reasons the event has not been included in Figure 1.

3.4. Decay time constant against solar event magnitude proxies

In an effort to understand the effect that event magnitudes may have on decays phases we produced plots of τ against CME speed, flare class, and SEP peak flux, $I_{p,25}^{max}$. These can be seen in Figures 9, 10, and 11. In Figure 9, CME speed is taken as the LASCO plane of sky (POS) speed for the associated CME for each event. Where multiple CMEs are associated with the event, the CME with the highest LASCO POS speed is used. Points are used if the spacecraft that took the particle measurements was connected within 35° to the event's associated AR. The constraint $|\Delta\phi| < 35^\circ$ is used to limit longitudinal effects on the plot and is used in Figures 10 and 11 as well. Only a weak correlation between CME speed and τ is seen (correlation coefficient, $cc = 0.49$). A faster CME may accelerate more particles over longer times resulting in long-duration decays. It may accelerate particles to higher energies lengthening decays as high energy particles decelerate to fill lower energy channels over time. The spatial extent over which energetic particles are found may be wider which combined with corotation may lengthen the decay.

In Figure 10, τ is plotted against the GOES soft x-ray flare class of each event. We see that τ has a stronger correlation to flare class ($cc = 0.69$) than we see for CME speed.

In Figure 11, SEP peak flux, $I_{p,25}^{max}$, is the largest peak event flux over all observing spacecraft within 35° , in the proton ~ 25 MeV channel. For all our events, we found that the maximum $I_{p,25}$ is associated with the closest connected spacecraft, having the minimum $\Delta\phi$ value. The proton ~ 25 MeV channel

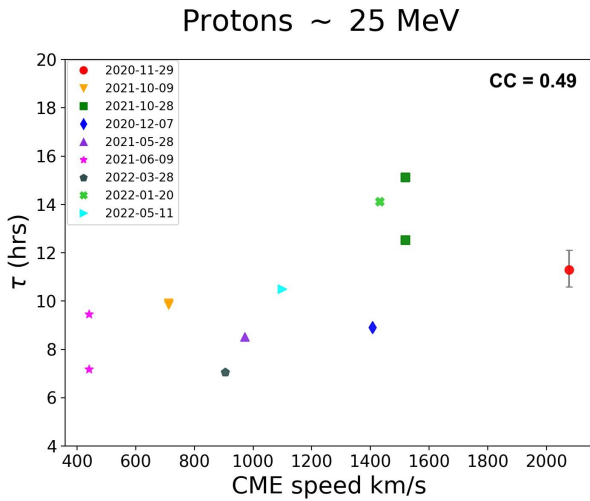


Fig. 9: Decay time constant against CME speed for protons ~ 25 MeV, for all spacecraft observations within $|\Delta\phi| < 35^\circ$. Where two spacecraft satisfy this condition, both data points are plotted for the same event. The CC value is the correlation coefficient.

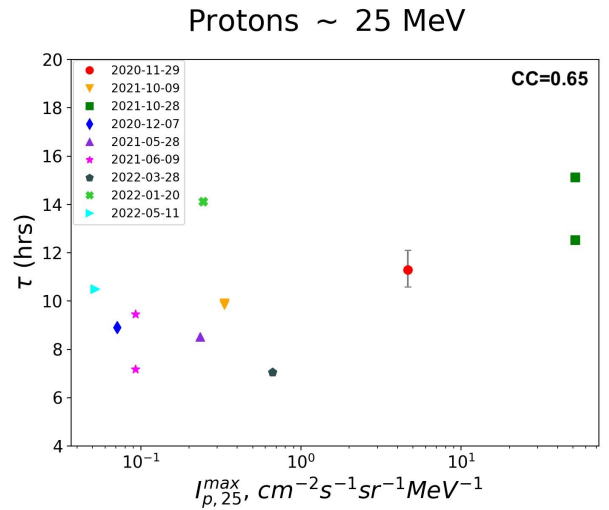


Fig. 11: Decay time constant against $I_{p,25}^{max}$, the maximum proton ~ 25 MeV SEP peak flux over all spacecraft within $|\Delta\phi| < 35^\circ$. The CC value is the correlation coefficient.

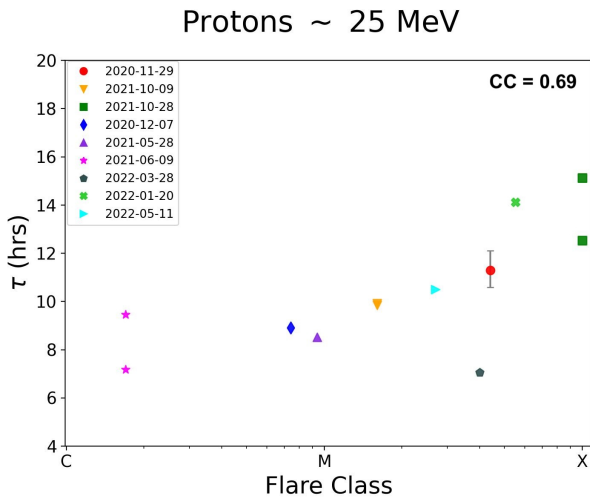


Fig. 10: Decay time constant against GOES soft x-ray flare class for protons ~ 25 MeV, for all spacecraft observations within $|\Delta\phi| < 35^\circ$. Where two spacecraft satisfy this condition, both data points are plotted for the same event. The CC value is the correlation coefficient.

is chosen as it has the most overlap across spacecraft instruments and is most reliable in obtaining measurements regardless of event magnitude. There is a weak trend for an increase in τ as $I_{p,25}^{max}$ increases (cc = 0.65). Nine out of twelve of the points are on the left-hand side of the graph, with $I_{p,25}^{max}$ of less than $1 \text{ cm}^{-2}\text{s}^{-1}\text{sr}^{-1}\text{MeV}^{-1}$. This leaves a cluster of points on the left-hand side, and a sparse set of points on the right-hand side.

3.5. Fitting late phase decay vs entire decay

The decay time constant values presented in Section 3 were derived by fitting intensities between 90% of I_p and the time that intensities reach background levels again. However, other choices are possible for the fit. Lario (2010) identified two phases in the decay of several events observed during solar cycle 23. In these

events, which tended to be well-connected events, they observed an initial, rapid, power-law decay phase, and a later, exponential decay phase. They chose to fit only the later exponential decay phase when deriving τ , which generally results in larger values of τ for these events compared to when the earlier decay phases are included.

We have analysed the effect of choosing to fit only the later phase of the event, by fitting intensities between 50% of I_p and the time when background is reached. Figure 12 shows the effect of this choice to be compared with Figure 1. There are some differences compared to Figure 1 but the main trends remain the same. Errors on the τ values are also larger in Figure 12 due to including fewer data points. Figure 13 shows the 50% of I_p version of Figure 3, and we see that the majority of the events follow the trend of decreasing τ values with increasingly western $\Delta\phi$ values. The two events with positive $\frac{d\tau}{d(\Delta\phi)}$ values in Figure 3 have slightly larger positive $\frac{d\tau}{d(\Delta\phi)}$ values in Figure 13, but are still in the minority. This shows that the east-west trend we see is not simply caused by the presence of an initial faster decay phase seen by observers with a closer connection to the acceleration region of the SEP event.

4. Discussion and Conclusions

In this work we have analysed 11 SEP events with 4 observing spacecraft with focus on the decay phase. We determined the decay time constant, τ , in two proton and one electron channel and studied its dependence on $\Delta\phi$, the longitudinal separation between the source AR and observer footprint location at the Sun.

The main results of this work are:

1. Within individual events there is a trend of decreasing τ values for increasingly western observers (τ decreasing with increasing $\Delta\phi$ (Figures 1 and 3)). This is seen for both electrons and protons, however more data points for higher energy protons are needed to investigate the consistency of the trend across different proton energies.
2. The east-west trend for individual events is present regardless of whether we fit the whole decay phase or only a later stage of the decay phases (Figure 12).

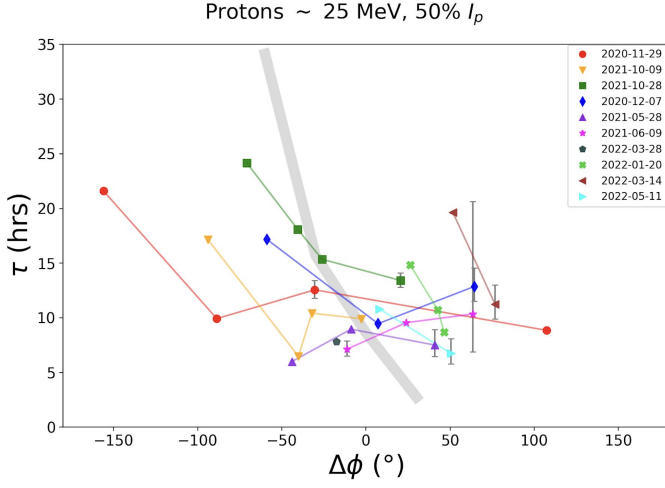


Fig. 12: Decay time constant τ versus longitudinal separation $\Delta\phi$ (as given by Equation 2) for ~ 25 MeV protons. The start of the decay phase is defined as when intensities return to 50% of I_p . Coloured lines connect s/c data points for a single event. Grey shading show results from a 25 MeV simulation run following the methodology of Hutchinson et al. (2023b). Error bars are omitted when they are smaller than the data points.

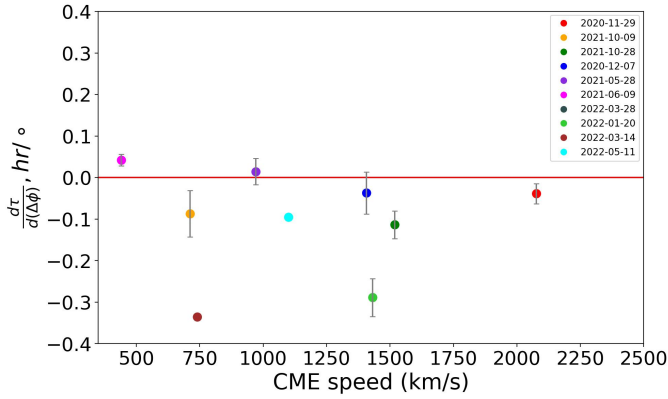


Fig. 13: Slope values from the linear fit of τ vs $\Delta\phi$ data points, for each event against CME speed. The start of the decay phase is defined as when intensities return to 50% of I_p .

3. The overall magnitude of the events has an effect on the value of τ (Section 3.2), and it is likely that transport conditions also play a role. There is a trend for τ to increase with flare class ($cc = 0.69$) and SEP peak flux ($cc = 0.65$), $I_{p,25}^{max}$, but the trend is weak for CME speed ($cc = 0.49$) (Figures 9 to 11).

The multi-spacecraft element of the analysis has been key to identifying a dependence of τ on $\Delta\phi$. Lario (2010) did not find a systematic dependence of τ on longitude. This may be because each point in their plot corresponds to a separate event and many parameters vary from event to event. For example, solar event magnitude (as discussed in Section 3.2) as well as solar wind and IMF conditions play an important roles in determining the τ value. It should be noted that for their plot of τ against longitude (their Figure 10), they used the longitude of the source AR as their x-axis. Thus they did not take into account possible effects of the solar wind speed on the magnetic connection of the observer. Our conclusion is that when only single spacecraft events are included in a study, the east-west trend is hidden by

the large variability in τ values in different events. In our analysis we try to derive $\Delta\phi$ values for the events as accurately as possible however these may be influenced by factors such as turbulence, field line meandering and coronal and interplanetary structures (Wimmer-Schweingruber et al. 2023).

Dalla (2003) used data from Helios 1 and 2 and IMP8 to study the dependence of event duration on $\Delta\phi$ for 52 gradual events. They found a trend for the longest durations to be associated with events with large negative $\Delta\phi$ and for events with large positive $\Delta\phi$ to have short durations. Since there is a correlation between duration and decay time constant, their results are consistent with those presented in Figure 1.

In addition to event magnitude already discussed, a number of other influences on decay time constants are likely to play a role. Previous studies have found effects of radial distance of the observing spacecraft from the Sun on decay phases. Kecskeméty et al. (2009) compared decay time constants for events at Helios 1 and 2 and IMP to those at Ulysses, covering radial ranges of ~ 1 -5 AU. They found that τ increased with increasing radial distance between 2-5 AU. A similar trend was found by Lario (2010). In our analysis, in order to separate observer longitude effects from observer radial effects, we chose to only include measurements of SEPs from spacecraft when they were located further than 0.6 AU from the Sun.

The east-west trend in τ values can be interpreted as a signature of corotation, guided by the results of simulations by Hutchinson et al. (2023a) who showed that corotation introduces a systematic decrease of τ with increasing $\Delta\phi$ compared to simulations that do not include corotation. An alternative possibility is that this trend is due to the temporal and spatial dependence of particle acceleration. In particular it has been suggested that variation in profile parameters with $\Delta\phi$ may be due to changes in the acceleration efficiency along a CME-driven shock front accelerating the particles (Reames et al. 1996). The way in which the energetic particle profiles at different observers are influenced by CME shock properties is discussed for example by Hu et al. (2017). Finally the presence of different interplanetary transport conditions at different longitudes may also explain different τ values although not a systematic decrease with $\Delta\phi$.

Hutchinson et al. (2023b) modelled a time-extended injection from a broad shock in the presence of corotation and showed that the measured intensity profiles at different observers depend only weakly on the characteristic of the injection at the shock (for example on whether the injection at the shock is gaussian or uniform). It is interesting to note that in the past fitting of the decay phase was used to determine the value of the scattering mean free path λ within 1D transport models. Hutchinson et al. (2023b) also showed that when corotation is included the decay time constant shows little dependence on the value of the scattering mean free path.

The simulations of Hutchinson et al. (2023a) did not include the effects of perpendicular transport on SEPs. By enabling particles to propagate across magnetic flux tubes as time goes on, perpendicular transport would be expected to reduce the signatures of corotation in the decay phase. This may explain why in the majority of events we studied, the gradient $\frac{d\tau}{d(\Delta\phi)}$ is less steep than in the simulations.

The test particle simulations in Hutchinson et al. (2023a) indicate that corotation has an important effect in shaping SEP decay phases and should be included in SEP models and interpretations of events. The systematic nature of the τ vs $\Delta\phi$ slopes observed in the events that we analysed appears to support the simulation results. In a separate study, Dalla et al. (2024) analysed the distribution of SEP event occurrence in $\Delta\phi$ and showed

the existence of an asymmetry in detection which could also be a signature of corotation. We conclude that corotation should be included in SEP models and interpretations of events, although other processes like acceleration and transport may be involved in producing the observed trends.

Future work should include a larger sample of events which will be made possible as solar cycle 25 continues and multi-spacecraft measurements continue to be taken. Future studies with a larger sample of events could also group events with similar parameters such as flare class and SEP peak flux. This may aid in reducing the spread of τ values seen and making an east-west trend clearer when events are viewed together.

Acknowledgements. R.H. acknowledges funding from the Moses Holden Studentship for her PhD. T.L. and S.D. acknowledge support from the UK Science and Technology Facilities Council (STFC) through grants ST/V000934/1 and ST/Y002725/1. A.H. would like to acknowledge support from the University of Maryland Baltimore County (UMBC), the Partnership for Heliophysics and Space Environment Research (PHaSER), and NASA/GFSC. We acknowledge use of solar energetic particle data from the SOHO, STEREO-A, Solo and PSP spacecraft and thank the instrument teams for their work on making the data available and science-ready. Solar Orbiter is a mission of international cooperation between ESA and NASA, operated by ESA. Thanks to the Integrated Science Investigation of the Sun (IS \odot IS) Science Team (PI: David McComas, Princeton University), and the Energetic Particle Detector (EPD) Team (PI: Javier Rodríguez-Pacheco, University of Alcalá, Spain). We acknowledge use of SERPENTINE tools, which were developed with funding from the European Union's Horizon 2020 research and innovation program, and of the Solar-MACH tool. The use of the data made available via the NSSDC CDAWeb is acknowledged.

References

- Cane, H. V., Reames, D. V., & Von Rosenvinge, T. T. 1988, *Journal of Geophysical Research: Space Physics*, 93, 9555.
- Dalla, S., Hutchinson, A., Hyndman, R. A., et al. 2024, arXiv:2411.08211
- Dalla, S. 2003, *Solar Wind Ten*, 679, 660.
- Daibog, E. I., Logachev, Y. I., & Kecskeméty, K. 2006, *Cosmic Research*, 44, 500.
- Domingo, V., Fleck, B., & Poland, A. I. 1995, *Solar Physics*, 162, 1.
- Dresing, N., Yli-Laurila, A., Valkila, S., et al. 2024, SERPENTINE catalog of solar cycle 25 multi-spacecraft solar energetic particle events. Events Catalog, S. 2024, SERPENTINE Events Catalog, <https://data.serpentine-h2020.eu/catalogs/sep-sc25/>.
- Fox, N. J., Velli, M. C., Bale, S. D., et al. 2016, *Space Science Reviews*, 204, 7.
- Giacalone, J. & Jokipii, J. R. 2012, *The Astrophysical Journal Letters*, 751, L33.
- Gieseler, J., Dresing, N., Palmroos, C., et al. 2023, *Frontiers in Astronomy and Space Sciences*, 9.
- Hu, J., Li, G., Ao, X., Zank, G. P., & Verkhoglyadova, O. 2017, *Journal of Geophysical Research: Space Physics*, 122, 10,938.
- Hutchinson, A., Dalla, S., Laitinen, T., & Waterfall, C. O. G. 2023a, *Astronomy & Astrophysics*, 670, L24.
- Hutchinson, A., Dalla, S., Laitinen, T., & Waterfall, C. O. G. 2023b, *Astronomy & Astrophysics*, 670, A178.
- Kaiser, M. L., Kucera, T. A., Davila, J. M., et al. 2008, *Space Science Reviews*, 136, 5.
- Kallenrode, M.-B. & Wibberenz, G. 1997, *Journal of Geophysical Research*, 102, 22311.
- Kallenrode, M. B., Wibberenz, G., & Hucke, S. 1992, *The Astrophysical Journal*, 394, 351.
- Kecskeméty, K., Daibog, E. I., Logachev, Y. I., & Kóta, J. 2009, *Journal of Geophysical Research (Space Physics)*, 114, A06102.
- Khoo, L. Y., Sánchez-Cano, B., Lee, C. O., et al. 2024, *The Astrophysical Journal*, 963, 107.
- Klein, K.-L. & Dalla, S. 2017, *Space Science Reviews*, 212, 1107.
- Laitinen, T., Dalla, S., Battarbee, M., & Marsh, M. S. 2018, 335, 298.
- Lario, D. 2010, *The Astrophysical Journal Supplement Series*, 189, 181.
- Lario, D., Sanahuja, B., & Heras, A. M. 1998, *The Astrophysical Journal*, 509, 415.
- McComas, D. J., Alexander, N., Angold, N., et al. 2016, *Space Science Reviews*, 204, 187.
- McCracken, K. G., Rao, U. R., Bukata, R. P., & Keath, E. P. 1971, *Solar Physics*, 18, 100.
- Müller, D., St. Cyr, O. C., Zouganelis, I., et al. 2020, *Astronomy and Astrophysics*, 642, A1.
- Müller-Mellin, R., Kunow, H., Fleißner, V., et al. 1995, *Solar Physics*, 162, 483.
- Palmroos, C., Gieseler, J., Dresing, N., et al. 2022, *Frontiers in Astronomy and Space Sciences*, 9.
- Reames, D. V., Barbier, L. M., & Ng, C. K. 1996, *The Astrophysical Journal*, 466, 473.
- Reames, D. V., Kahler, S. W., & Ng, C. K. 1997, *The Astrophysical Journal*, 491, 414.
- Rodríguez-García, L., Gómez-Herrero, R., Dresing, N., et al. 2024, Solar energetic particles injected inside and outside a magnetic cloud: The widespread solar energetic particle event on 2022 January 20.
- Rodríguez-Pacheco, J., Wimmer-Schweingruber, R. F., Mason, G. M., et al. 2020, *Astronomy & Astrophysics*, 642, A7.
- Torsti, J., Valtonen, E., Lumme, M., et al. 1995, *Solar Physics*, 162, 505.
- Valtonen, E., Peltonen, J., Peltonen, P., et al. 1997, *Nuclear Instruments and Methods in Physics Research A*, 391, 249.
- Van Allen, J. A. & Krimigis, S. M. 1965, *Journal of Geophysical Research (1896-1977)*, 70, 5737.
- von Rosenvinge, T. T., Reames, D. V., Baker, R., et al. 2008, *Space Science Reviews*, 136, 391.
- Wimmer-Schweingruber, R. F., Berger, L., Kollhoff, A., et al. 2023, *Astronomy & Astrophysics*, 678, A98.

Table .1: Associated flare and CME properties for SEP events analysed. Event date and flare onset time and location are given. These times and locations are taken from the SERPENTINE Events Catalog (Dresing et al. 2024). Entries marked with * are taken from Khoo et al. (2024) rather than the SERPENTINE catalogue due to data availability. Event magnitude proxies such as flare class, CME speed and maximum peak flux, $I_{p,25}^{max}$, values are given. Flare classes and $I_{p,25}^{max}$ values are also taken from SERPENTINE. $I_{p,25}^{max}$ values are the maximum proton peak flux for the ~ 25 MeV channel, across the 4 observing spacecraft we use. CME speeds are plane of sky speeds from LASCO. Where more than one CME is associated, the largest plane of sky LASCO value is used.

Event Date	Spacecraft	$\Delta\phi$, °	Radial distance, au	τ_{E1}	τ_{P25}	τ_{P60}	$\frac{d\tau}{d(\Delta\phi)}$, hrs/°	Error on $\frac{d\tau}{d(\Delta\phi)}$
29/11/2020	SOHO	-156.0	0.98	30.8	22.7	-	-0.0624	0.0265
-	STEREO-A	-88.6	0.96	12.3	10.2	-	-	-
-	PSP	-30.4	0.81	15.3	11.3	-	-	-
-	Solo	107.4	0.88	15.6	8.9	6.6	-	-
07/12/2020	SOHO	-58.9	0.98	-	19.0	-	-0.0912	0.0638
-	STEREO-A	7.2	0.96	-	8.9	4.5	-	-
-	PSP	64.5	0.78	-	12.9	-	-	-
-	Solo	-161.0	0.84	-	-	-	-	-
28/05/2021	SOHO	-8.9	1.00	5.7	8.5	-	-0.0071	0.0293
-	STEREO-A	41.0	0.96	-	6.9	-	-	-
-	PSP	-44.0	0.69	8.2	5.9	-	-	-
-	Solo	87.8	0.95	-	-	-	-	-
09/06/2021	SOHO	23.9	1.01	6.6	9.5	-	-0.0149	0.0267
-	STEREO-A	63.6	0.96	-	8.4	-	-	-
-	PSP	-11.2	0.76	-	7.2	-	-	-
-	Solo	135.7	0.95	-	-	-	-	-
09/10/2021	SOHO	-93.9	0.99	15.8	18.3	-	-0.1146	0.0624
-	STEREO-A	-32.1	0.96	4.1	9.9	4.6	-	-
-	PSP	-2.8	0.77	7.7	9.9	-	-	-
-	Solo	-40.1	0.68	3.9	6.2	3.7	-	-
28/10/2021	SOHO	-70.8	0.98	24.9	30.6	17.9	-0.2242	0.0737
-	STEREO-A	-26.1	0.96	16.5	15.1	12.3	-	-
-	PSP	20.5	0.62	19.5	12.5	-	-	-
-	Solo	-40.5	0.80	21.5	17.4	13.9	-	-
20/01/2022	SOHO	26.3	0.98	14.3	14.1	5.7	-0.2874	0.0585
-	STEREO-A	42.8	0.97	8.8	10.3	7.1	-	-
-	PSP	-177.6	0.73	-	-	-	-	-
-	Solo	46.4	0.92	7.9	8.1	6.1	-	-
15/02/2022	SOHO	160.4	0.98	-	68.5	-	-	-
-	STEREO-A	-179.0	0.97	38.6	39.2	32.7	-	-
-	PSP	-8.5	0.38	-	-	-	-	-
-	Solo	-175.5	0.72	53.4	-	-	-	-
14/03/2022	SOHO	51.6	0.98	8.6	19.8	-	-0.357	0.0
-	STEREO-A	76.7	0.97	-	10.8	-	-	-

Continued on next page

Table .1 – continued from previous page

Event Date	Spacecraft	$\Delta\phi, ^\circ$	Radial distance, au	τ_{E1}	τ_{P25}	τ_{P60}	$\frac{d\tau}{d(\Delta\phi)}, \text{ hrs}/^\circ$	Error on $\frac{d\tau}{d(\Delta\phi)}$
-	PSP	-49.2	0.53	-	-	-	-	-
-	Solo	64.6	0.41	-	-	-	-	-
28/03/2022	SOHO	-47.6	0.99	7.4	10.9	6.3	-0.1269	0.0
-	STEREO-A	-17.5	0.97	5.6	7.1	5.4	-	-
-	PSP	-166.7	0.69	-	-	-	-	-
-	Solo	-111.6	0.33	-	-	-	-	-
11/05/2022	SOHO	8.0	1.00	8.6	10.5	-	-0.1146	0.0
-	STEREO-A	50.6	0.96	-	5.6	-	-	-
-	PSP	-67.6	0.59	-	-	-	-	-
-	Solo	-128.2	0.79	-	-	-	-	-